

Observation of Fatigue Crack Initiation and Growth in Stainless Steel to Quantify Low-Cycle Fatigue Damage for Plant Maintenance

Masayuki KAMAYA^{1,*}

¹ *Institute of Nuclear Safety System, Inc., 64 Sata, Mihama-cho, Fukui 919-1205, Japan*

ABSTRACT

Quantifying the low-cycle fatigue damage accumulated in nuclear power plant components is one of the important issues for aged plants. In this study, detailed observations of crack initiation and growth were made using scanning electron microscopy in order to correlate the crack size and the magnitude of the fatigue damage. Type 316 stainless steel specimens were subjected to the strain-controlled axial fatigue test (strain range: 1.2%) in air at room temperature. The test was interrupted several times in order to observe the specimen surface. The spatial distribution of inhomogeneously accumulated damage by cyclic loading was identified by crystal orientation measurements using the electron backscatter diffraction technique. Cracks were initiated at grain boundaries and slip steps, where relatively large damage accumulated. The changes in the number of cracks and their length were quantified. The crack growth rates were well correlated with the strain intensity factor. The change in crack size during the fatigue test was predicted using the obtained growth rate and assumed initial crack size. The fatigue lives estimated by the crack growth prediction agreed well with those obtained experimentally. It was concluded that the fatigue damage could be estimated from the crack size measured in plant components.

KEYWORDS

low-cycle fatigue, fatigue damage, crack growth, fatigue life, life prediction, stainless steel, strain intensity factor

ARTICLE INFORMATION

Article history:

Received 17 June 2013

Accepted 2 September 2013

1. Introduction

In the structural design of nuclear power plant components, fatigue damage has been assessed by quoting a usage factor (UF) [1], which is accumulated fatigue damage according to the linear damage accumulation rule. Nowadays, due to long time operation over forty years for some plants, UF may exceed the critical value for some components. Even if UF exceeds the critical value, however, the components may not be always damaged because sufficient margins were considered in the design. It is difficult to judge whether the components of interest are actually damaged or not from surface observations or inspections. It is important to correlate the fatigue damage to a material change which can be measured in order to quantify the fatigue damage accumulated in the components.

In order to quantify the fatigue damage, it is important to understand what kind of change is brought about by cyclic loading, and to know the critical conditions for fatigue life. Using carbon steel (S45C) specimens, Murakami and Miller [2] showed that crack initiation and growth could be regarded as the damage caused by fatigue loading and that fatigue life was almost equivalent to the number of cycles for the initiated cracks growing to the critical size. Other researchers showed that the remaining fatigue life of damaged specimens was recovered by removing cracks initiated on the specimen surface for carbon steel [3][4] and stainless steel [5]. The fatigue loading causes various microstructural changes such as an increased number of dislocations, formation of cell structures, and alternation of deformation properties. However, these changes have minor influence on the fatigue life under the same strain range. Therefore, the fatigue damage can be correlated to the crack size. It is possible to measure (quantify) the fatigue damage by investigating the size of a crack initiated in components, or if no crack is found, it can be confirmed that damage has not been accumulated yet.

*Corresponding author, E-mail: kamaya@inss.co.jp

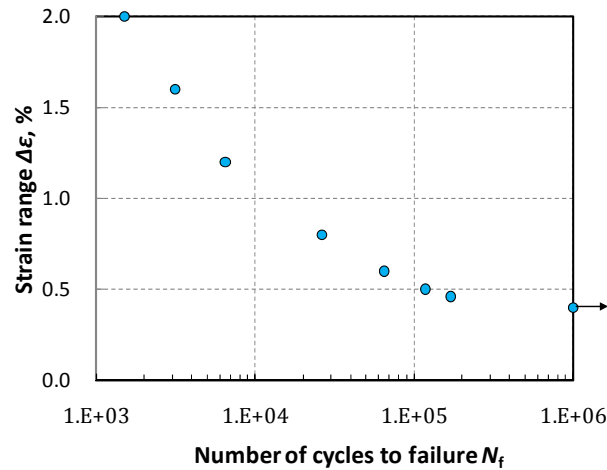


Fig. 1 Fatigue lives of Type 316 stainless steel specimens obtained from the strain-controlled fatigue test done in air at room temperature [22].

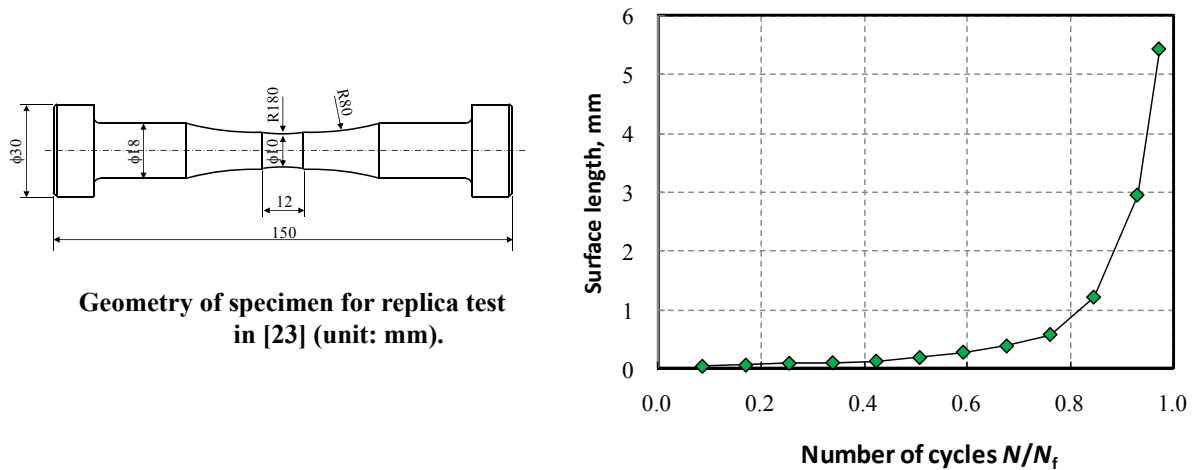


Fig. 2 Change in surface length obtained under constant cyclic strain of $D\epsilon = 1.2\%$ [23].

The fatigue life can be divided into two phases: the number of cycles to crack initiation (hereafter called initiation life) and the remaining life until the failure of the specimen (hereafter called growth life). It was shown that cracks tens of microns in length were initiated at less than 10% of the total fatigue life [6]. Therefore, by assuming a small size for predicting the growth life, it is possible to neglect the initiation life for the fatigue life estimation. It is relatively easy to quantify the growth life because the crack growth rate has been shown to correlate with the stress intensity factor (SIF), and the experimental technique for obtaining the material constants for growth prediction has been standardized [7]. Extensive attempts have been made to estimate the fatigue life by integrating the crack growth [8-12]. For the low-cycle fatigue regime, in which cyclic plastic strain is significant and SIF is not valid for representing the crack growth driving force, the prediction using the J-integral value [13-15] or the strain intensity factor [15-17] was shown to be valid for the growth prediction. For predicting small crack growth, it is important to consider the scatter in the growth rate. It was pointed out that the growth rate of microstructurally small cracks was changed due to microstructures such as grain boundaries [18][19]. The inhomogeneous stress and strain distribution at the microstructural scale also affected the growth rate [20][21], although its influence decreased as the crack size increases. For a precise fatigue life prediction, it is important to characterize how the growth rate is changed depending on the crack size.

The main objective of this study was to quantify the fatigue damage by crack size identification. In order to achieve this objective, crack initiation and growth behavior during the low-cycle fatigue test were observed for Type 316 stainless steel specimen. The strain-controlled axial fatigue test was

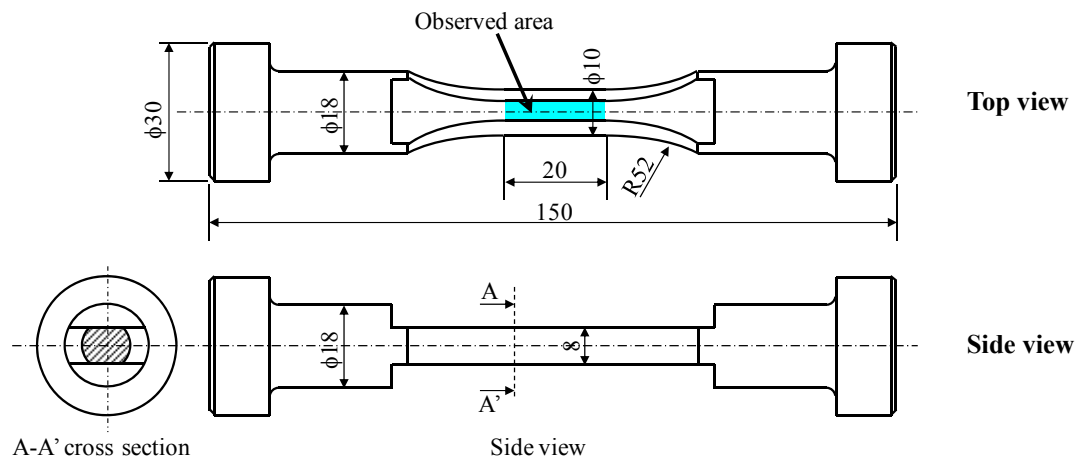


Fig. 3 Geometry of test specimen (unit: mm).

conducted in room temperature laboratory environment. The specimen surface was observed by using scanning electron microscopy (SEM) by interrupting the test at regular cycle intervals. This allowed observations of cracks of a few microns and their interaction with the microstructure. The electron backscattered diffraction (EBSD) measurements were made to correlate the crack initiation to grain boundaries and inhomogeneity of local deformation. Then, the growth rates and their correlation with the fatigue life were discussed. Finally, the correlation between the crack size and fatigue damage was shown.

2. Test Material and Procedure

2.1 Material and basic fatigue properties

The material used for the fatigue test was solution heat-treated Type 316 austenitic stainless steel, which was provided in a cylindrical bar shape. Its chemical composition (in mass%) was: C, 0.06; Si, 0.50; Mn, 1.30; P, 0.031; S, 0.027; Ni, 10.18; Cr, 16.94; Mo, 2.02 and balance Fe. The average 0.2% proof strength, tensile strength, elongation and Young's modulus from two tensile test runs at room temperature were 297 MPa, 611 MPa, 0.58 and 202,500 MPa, respectively. The material had an approximately equiaxial grain structure with an average grain diameter of 50 μm .

Figure 1 shows the fatigue life of the material obtained in a previous study [22], in which the strain controlled fatigue tests was conducted in a room temperature laboratory environment using cylindrical specimens. Strain range $\Delta\varepsilon$ was changed from $\Delta\varepsilon = 0.4\%$ to 2.0% under the constant strain rate of 0.4%/s. The estimated fatigue limit was 0.4% in the strain range.

The main crack growth behavior has been investigated for this material by conducting a strain-controlled fatigue test for the strain range of $\Delta\varepsilon = 1.2\%$ in a room temperature laboratory environment [23]. The crack growth during the test was monitored by taking replicas of the specimen surface using acetylcellulose films. The replica measurements were made almost every 500 cycles and the change in the surface length is shown in Fig. 2. The number of cycles was normalized by the fatigue life, which was $N_f = 5937$. A crack of 41.2 μm length was observed at $N = 500$ ($N/N_f = 0.09$), then it grew continuously and the growth rate accelerated as the crack size increased. In the present study, this test is referred to as the replica test.

2.2 Procedure

The geometry of the specimen used for the fatigue test is shown in Fig. 3; this test specimen was made from a cylindrical bar specimen by wire cutting. The specimen was subjected to the

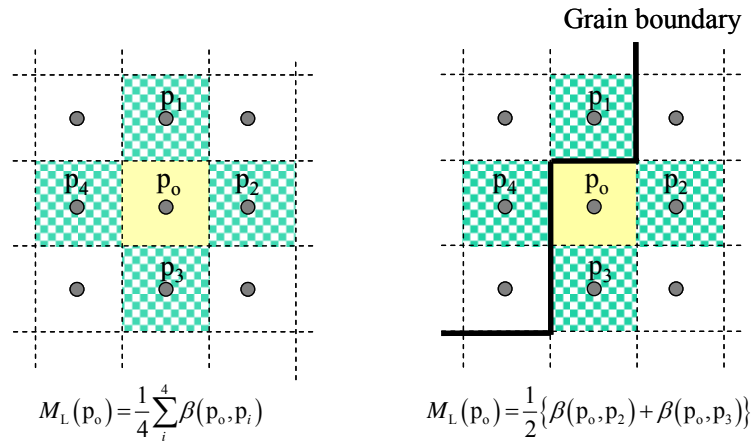


Fig. 4 Definition of local misorientations.

strain-controlled fatigue test of $\Delta\varepsilon = 1.2\%$ in ambient air at room temperature. Cracks were initiated on the flat surface, which is indicated as the “observed surface” in Fig. 3, and they were observed periodically by interrupting the test. The observed area was finished using 3 μm diamond paste followed by electropolishing in order to prepare for obtaining the EBSD pattern.

The surface observation was made using a field emission electron gun SEM (Carl Zeiss ULTRA55) at the number of cycles N of $N = 1000, 2000, 3000, 4000$ and 4400 . Although the fatigue life for $\Delta\varepsilon = 1.2\%$ was approximately 6000 for this material, it was difficult to continue to apply the cyclic strain at N over 4400 because the size of the main crack initiated at the edge of the polished area had become large. The area of a single observation was $500 \times 500 \mu\text{m}^2$. The secondary electron images were recorded with nine photos, in which the magnification was about $\times 600$, for each area. Seven areas, which are referred to as “traced areas” in this study, were observed continuously and an additional six areas, which are referred to as “non-traced areas”, were observed only at $N = 4400$.

Crystal orientations were measured for the traced and non-traced areas in order to investigate grain boundaries and local deformation caused by the cyclic loading and their correlation with crack initiation and growth behavior. These measurements were made only at $N = 1000$ in order to suppress the influence of initiated cracks on the crystal orientation measurements. The local misorientation distribution might be influenced by the stress and strain concentration near crack tips. The crystal orientations were measured by scanning over the areas with the step size of $1 \mu\text{m}$ using the commercial software, OIM Data Collection ver. 5.2. Based on the measured crystal orientations, the local change in crystal orientation (hereafter called local misorientation), M_L , was calculated by [24]:

$$M_L(p_0) = \frac{1}{4} \sum_{i=1}^4 \beta(p_0, p_i) \quad (1)$$

where $\beta(p_0, p_i)$ denotes the misorientation between a fixed point p_0 and neighboring points p_i as shown in Fig. 4. A line was drawn between two adjacent points when the misorientation was larger than 5° . If a series of the lines formed a closed region, the lines were defined as a grain boundary, and the misorientation between the points of different grains was not included in the calculation of M_L . A filtering process [25] was applied to reduce meaningless error in misorientation identification. The orientation data were analyzed using the in-house software MADAM (Misorientation Analyzer for DAmage Measurement) [26].

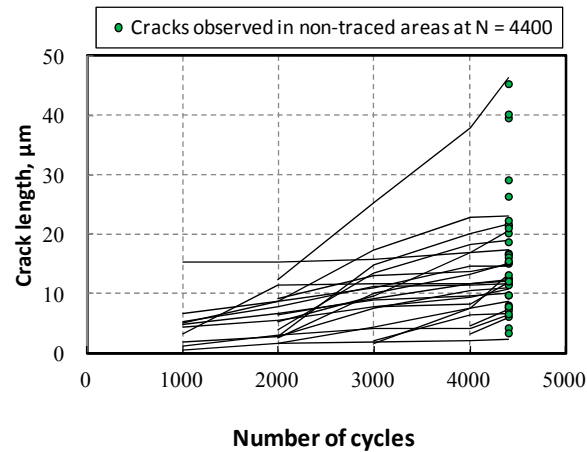


Fig. 5 Changes in crack length with number of cycles (number of cracks at $N = 4400$: 23 in traced areas and 34 in non-traced areas).

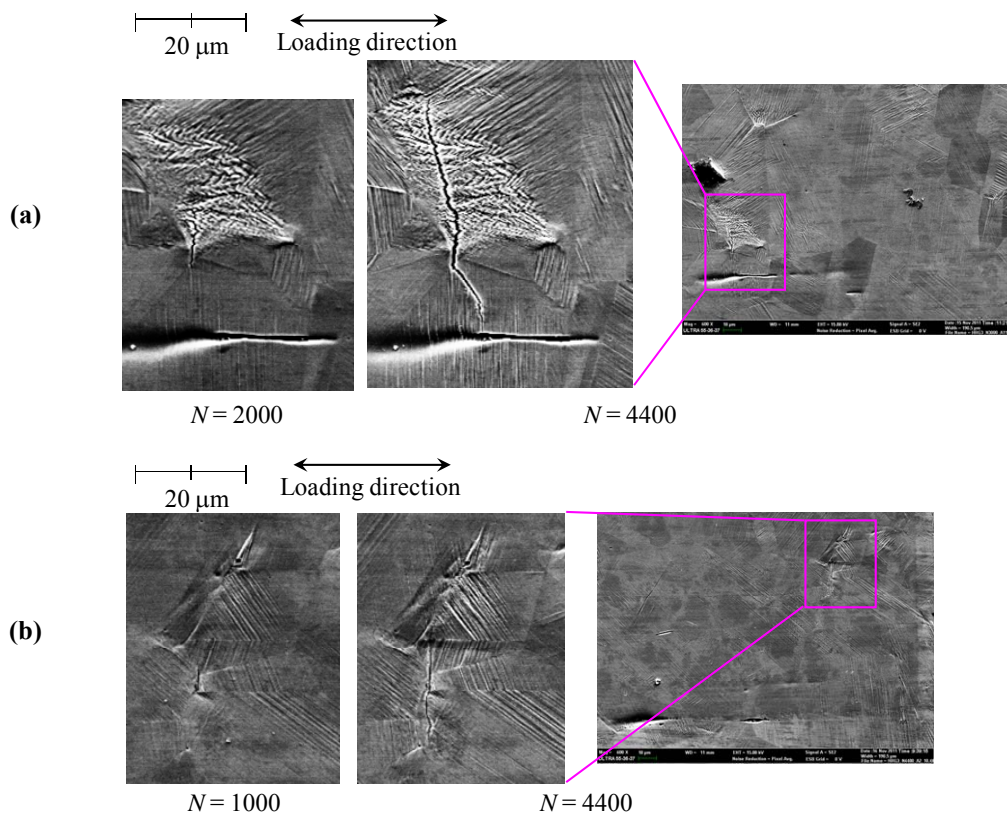


Fig. 6 Surface images observed by SEM.

3. Test Results

3.1 Observations of crack initiation and growth behavior

Changes in crack length are shown in Fig. 5. The number of cracks observed in the traced areas was 10 at $N = 1000$, and it increased to 23 at $N = 4400$. The maximum lengths were $15.2 \mu\text{m}$ and $46.4 \mu\text{m}$ at $N = 1000$ and 4400 , respectively. Additionally 24 cracks were observed at $N = 4400$ in the non-traced areas.

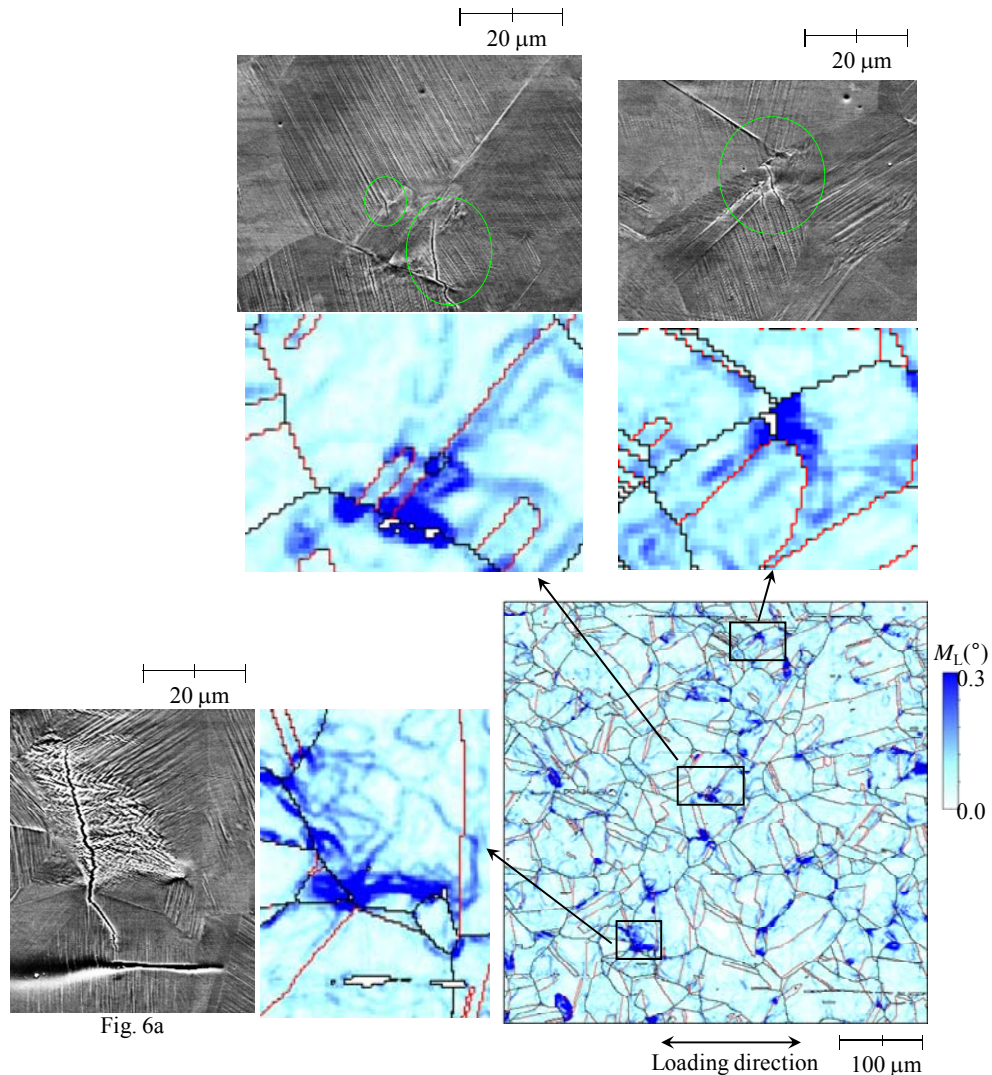


Fig. 7(a) Local misorientation obtained by EBSD measurements at $N = 1000$ and corresponding surface images observed at $N = 4400$. Red lines indicate twin boundaries and black lines show non-twin boundaries

Figure 6(a) shows surface images of the maximum crack at $N = 4400$, which had a length of $46.4 \mu\text{m}$. The crack was initiated at a junction of grain boundaries (hereafter, this is called the triple point) and grew transgranularly in a direction almost perpendicular to the loading direction. The surface roughness was relatively large near the area of the crack initiation. Fig. 6(b) shows surface images of another crack at $N = 4400$, which had a length of $23.1 \mu\text{m}$. Although many slip steps appeared on the surface around the crack, the crack was not initiated from the slip steps.

The position of grain boundaries could be identified by comparing SEM results (Fig. 6) with the EBSD measurement results. Figures 7(a) and (b) show the local misorientations together with the surface images near cracks observed at $N = 4400$. It should be noted again that the crystal orientations were measured at $N = 1000$, although the surface images correspond to $N = 4400$. It was found that the crack shown in Fig. 6(b) was initiated from the grain boundary, although it might have been initiated at a triple point originally. All cracks shown in Fig. 7 were initiated at grain boundaries, which included twin boundaries and triple points, and grew almost perpendicular to the loading direction. Thus, so-called stage I initiation (initiation due to shear stress) did not seem to be predominant.

The local misorientations exhibited an inhomogeneous distribution. The areas of large local misorientations were observed and spacing of such areas was about $100 \mu\text{m}$. In this study, the area of relatively large local misorientations was referred to as a “hot spot”. The cracks observed in Fig. 7

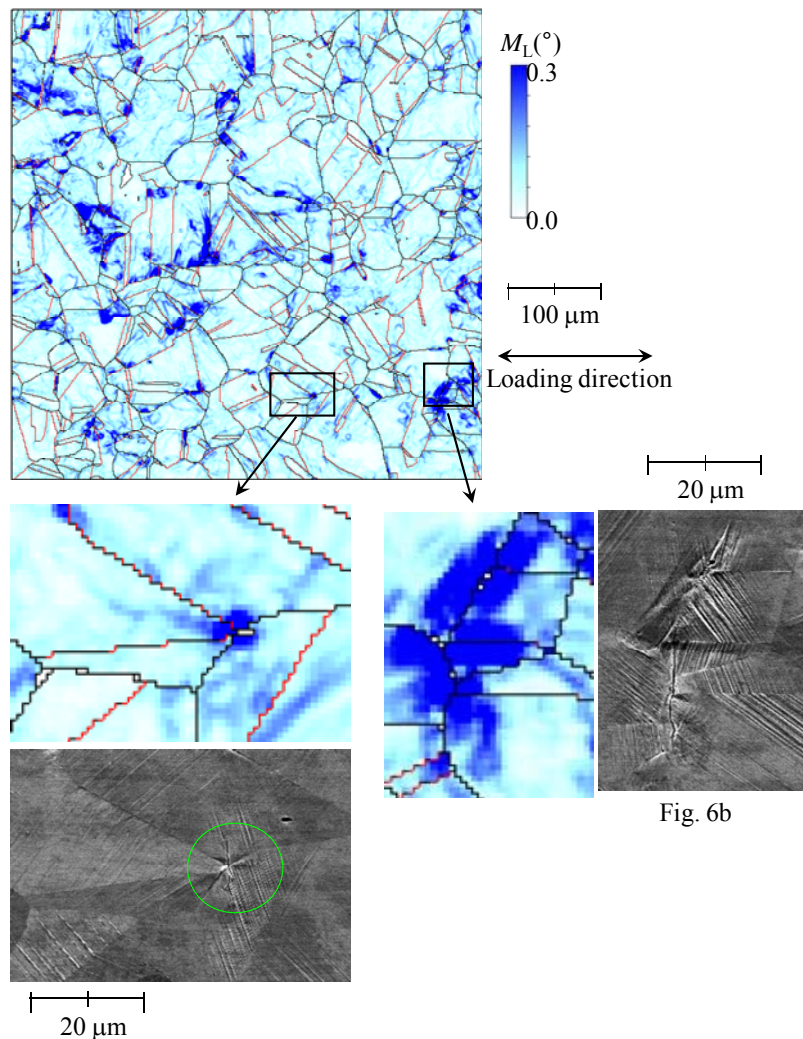


Fig. 6b

Fig. 7(b) Local misorientation obtained by EBSD measurements at $N = 1000$ and corresponding surface images observed at $N = 4400$. Red lines indicate twin boundaries and black lines show non-twin boundaries

were initiated at hot spots. The stress and strain distribution shows microstructural inhomogeneity in polycrystalline material. This causes the inhomogeneous deformation and results in the scattered hot spot distribution. It has been shown that the hot spots are brought about by high dislocation density [27-33] and localized deformation [34]. In the present specimen, the relatively large local misorientations near grain boundaries were attributed to pile-up of dislocations at the grain boundaries caused by gliding of slip steps. The cracks were initiated at such grain boundaries, although not all the hot spots initiated cracks.

3.2 Sites of crack initiation

The locations of the crack initiation were categorized into four sites: triple point, grain boundary (excluding the twin boundary), twin boundary and intra-grain, which are schematically shown in Fig. 8. As seen in Figs. 6 and 7, it was difficult to distinguish the triple point and grain boundary sites in some cases, and these might not be categorized exactly.

Figure 9 shows the change in the number of cracks initiated in the traced areas for each initiation site and the number of cracks at $N = 4400$ counted for all areas (traced and non-traced areas). "Others" denotes the cracks for which an initiation site could not be identified. The number of cracks initiated from triple points increased continuously, although the other initiation sites showed a relatively small change in the number of cracks initiated. Almost half of the cracks were initiated from triple points

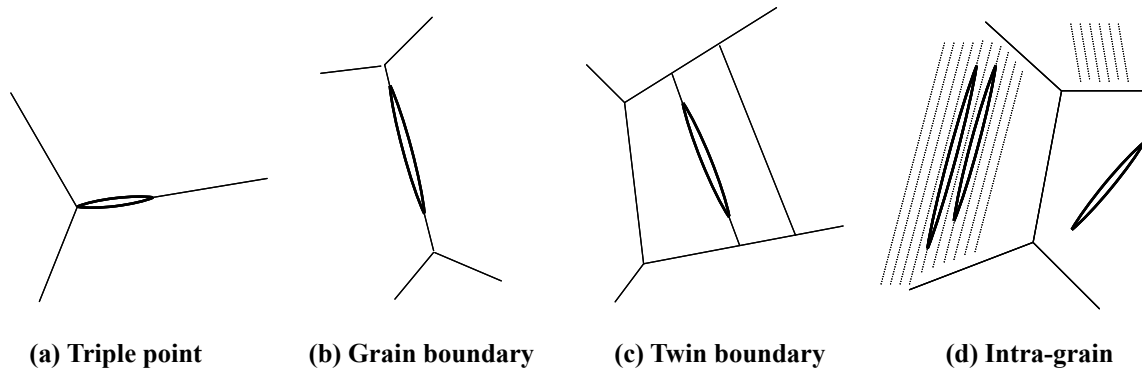


Fig. 8 Schematic drawings of crack initiation sites due to low-cycle fatigue.

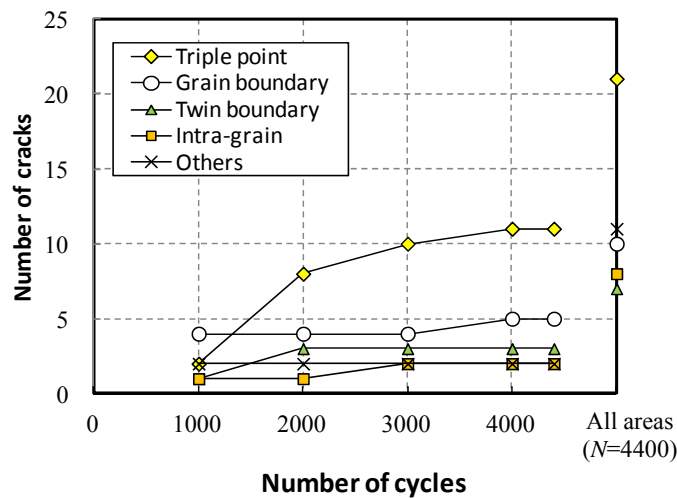


Fig. 9 Change with the number of cycles for the number of cracks for each initiation site.

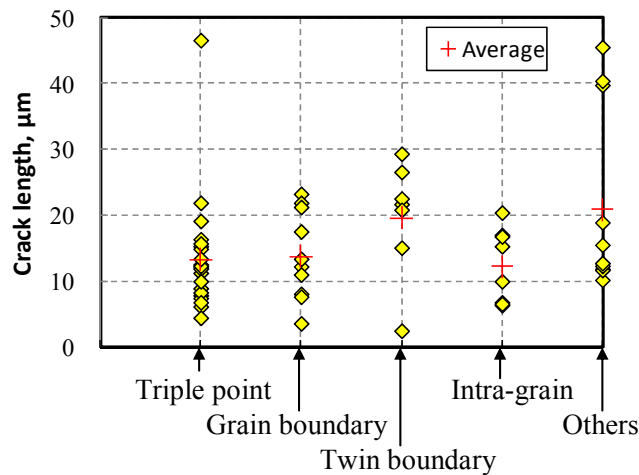


Fig. 10 Crack length of individual cracks and average length at $N = 4000$.

and grain boundaries. Therefore, grain boundaries, including triple point and twin boundaries, were the preferential site for the crack initiation of this material for $\Delta\varepsilon = 1.2\%$. It has been pointed out that grain boundaries could be susceptible to cracking in the low-cycle fatigue regime [35-37]. The resistance to crack initiation was deduced to be weakened at grain boundaries due to geometrical incompatibility caused by adsorbed dislocations. On the other hand, the intra-grain site cracks were initiated from a geometrically discontinuous part, such as slip steps or a roughened surface. The stress

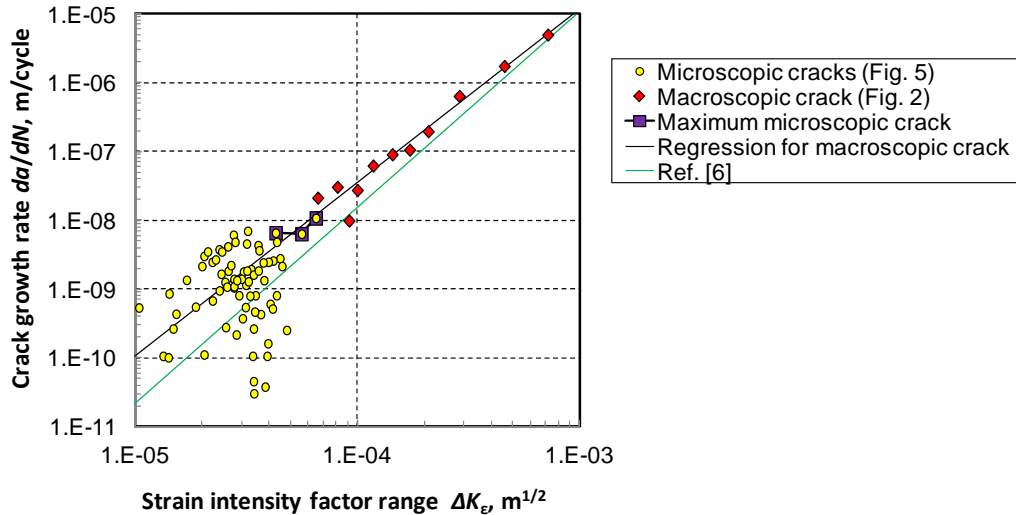


Fig. 11 Relationship between strain intensity factor and crack growth rates.

and strain concentration at the geometrical discontinuity enhances the driving force for crack initiation.

The crack length at $N = 4400$ is shown in Fig. 10 for each initiation site. Although the maximum size crack was initiated from a triple point, the cracks initiated from triple points were relatively short in length because these cracks were initiated from a point in the triple point initiation site. However, the cracks from triple points seemed to easily propagate into the grain perpendicular to the loading direction, and that resulted in the maximum crack at $N = 4400$. On the other hand, the length of the cracks initiated at twin boundaries was almost equivalent to that of the boundary length at the beginning. However, since twin boundaries were not always perpendicular to the loading direction and it would be difficult for a crack to change its growth direction at the triple point; cracks that initiated at twin boundaries did not always grow at a fast rate.

2.1. Crack growth rates

Crack growth rates in the depth direction were calculated from the inclination of the lines shown in Figs. 2 and 5, assuming the crack shape was the ratio of the depth to surface length, 0.5. Figure 11 shows the relationship between the crack growth rates in the depth direction and the range of the strain intensity factor (ΔK_ε), which is defined by:

$$\Delta K_\varepsilon = f \Delta \varepsilon \sqrt{\pi a}, \quad (2)$$

where $\Delta \varepsilon$ is the applied strain range (1.2%) and a is the crack depth. f is the geometrical constant for SIF which was obtained from Ref. [38] assuming cracks were small enough to ignore the boundary effect. It has been shown that the crack growth rate correlates well with the strain intensity factor even in low-cycle fatigue regime [14-16]. The correlation between the crack growth rates and SIF in the low-cycle regime was reported to have significant scatter due to relatively large cyclic inelastic strain [6]. The green line in Fig. 11 indicates the regression of growth rates obtained in the previous study [6], in which the same material was used, and it is expressed by:

$$\frac{da}{dN} = 3.94 \times 10^3 (\Delta K_\varepsilon)^{2.85} \quad (3)$$

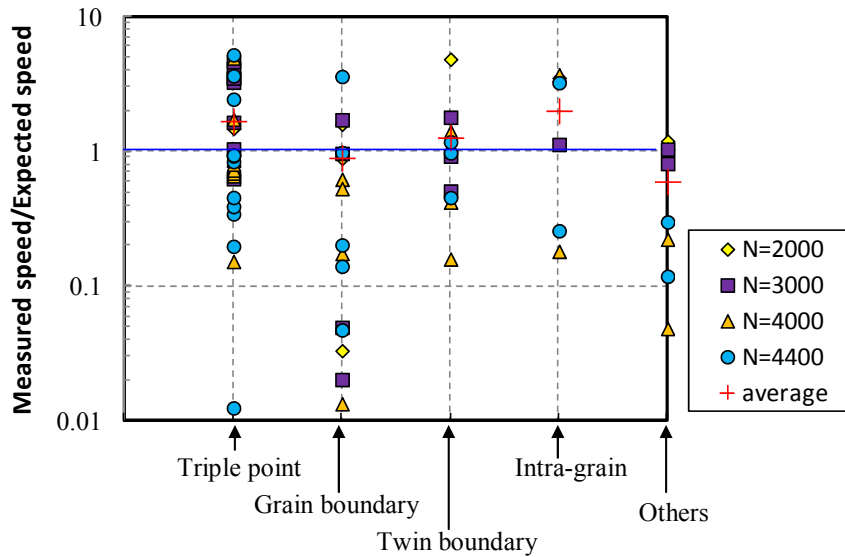


Fig. 12 Crack growth rates normalized by rate obtained from the regression curve of the macroscopic crack.

where growth rate is given in m/cycle and ΔK_e in $m^{0.5}$. The crack observed in the replica test (hereafter, the macroscopic crack) and cracks observed by SEM (hereafter, the microscopic cracks) had a similar growth rate to Eq. (3), although the microscopic crack growth rates showed significant scatter. The maximum crack at $N = 4400$ had a relatively fast growth rate compared with the other microscopic cracks and had almost the same regression curve as the macroscopic crack growth rates.

Figure 12 shows the growth rates for each initiation site normalized by the rate obtained from the regression curve of the macroscopic crack that was indicated by black solid line in Fig. 11. The means of the normalized growth rates were larger than unity, except for the initiation site of grain boundary. The stress or strain distribution is not homogeneous on a microscopic scale and the hot spots were deduced to be generated in a region of relatively large stress or strain. The microscopic cracks were initiated at, and grew in, the hot spots; these hot spots were typically several tens of microns. Therefore, the growth rate of the microscopic cracks, whose length was less than $46.4 \mu\text{m}$, grew in the hot spots. This could be the reason for their relatively fast growth rate. On the other hand, the inclination of the crack face was not always perpendicular to the loading direction, and this could reduce the growth rate particularly for the cracks initiated from the grain and twin boundaries. Furthermore, cracks initiated at grain boundaries have to change their growth direction when the crack tip hits a triple point. Such a kink in the crack tip reduces the driving force of the crack growth [39]. If the crack size becomes large and the number of grains along the crack front increases, the local change in crack growth direction at an individual triple point has only a small influence on the driving force of the whole crack. Then, the growth rates of the microscopic cracks were saturated to that of the macroscopic crack. The cracks initiated at the triple point and intra-grain sites showed relatively fast growth rates. The cracks of both sites tended to grow transgranularly perpendicular to the loading direction without retardation at grain boundaries.

4. Discussion

4.1 Initiation and growth of the macroscopic crack

The results shown in Figs. 2 and 5 are shown together in Fig. 13. The lengths of the macroscopic crack were larger than those of the microscopic cracks for the same number of cycles. Since the average growth rates of the microscopic cracks were comparable to those of the macroscopic crack the difference in the crack length was brought about by the initial crack size. The macroscopic crack length was $41.2 \mu\text{m}$ at $N = 500$, although the maximum was $15.2 \mu\text{m}$ for the microscopic cracks even when $N = 1000$. Figure 14 shows SEM images of the macroscopic

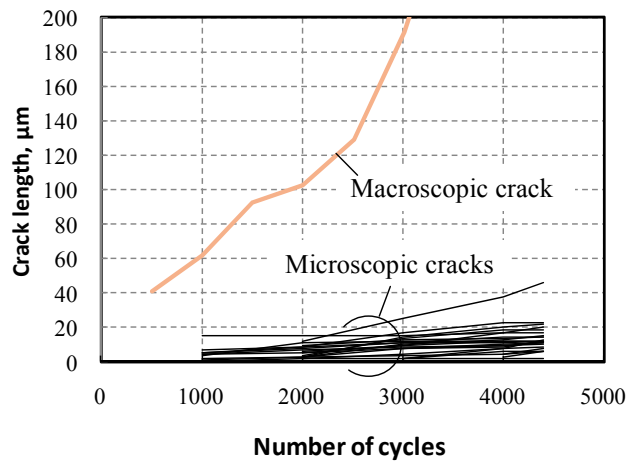


Fig. 13 Changes in crack length with number of cycles obtained from Figs. 2 and 5.

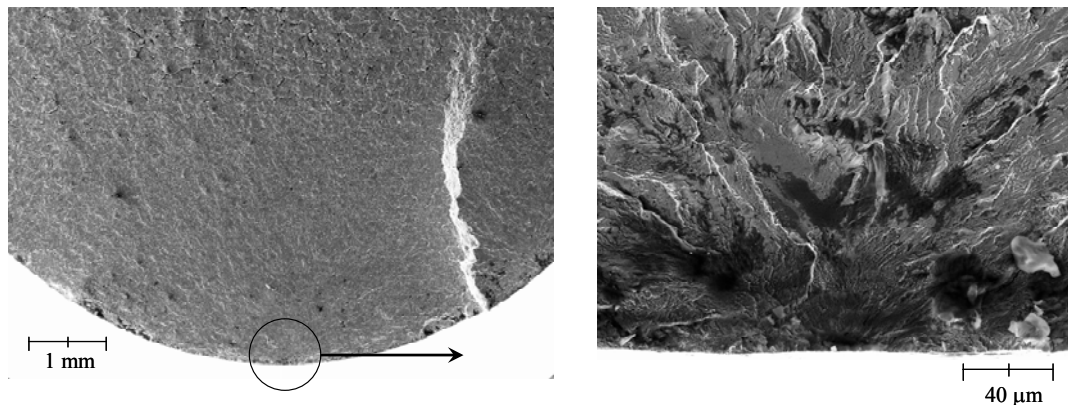


Fig. 14 SEM micrographs of the fractured surface of a fatigue test specimen to observe the origin of crack initiation (macroscopic crack shown in Fig. 2).

crack on the fractured surface. The magnified view of the origin of crack initiation showed a peculiar fracture pattern area with a radius of about 40 µm. It was difficult to identify the type of initiation site shown in Fig. 8.

It is reasonable that the maximum crack length of the microscopic cracks was smaller than that of the macroscopic crack, because the microscopic crack were observed only in the traced areas while the macroscopic crack was the maximum crack that appeared in the whole specimen. The larger area would have more chances to initiate larger cracks. The expected microscopic crack size for the larger observation area was estimated by Gumbel statistics. Figure 15 shows the Gumbel probability plot for the maximum crack length at $N = 1000$ for each traced area. The solid line shows the regression of the maximum length for each area. The Gumbel plot enables prediction of the expected maximum crack length by extrapolating the regression line. If the surface area for the macroscopic crack is taken as $10\pi \times 12 \text{ mm}^2$, this size was about 1508 times larger than that of the traced area, which was 0.25 mm^2 . Then, the reduced variable y in Fig. 15 could be derived by setting cumulative probability F equal to $F = 1508/(1508+1)$, and the corresponding maximum crack length was 26.9 µm. However, the estimated maximum crack length was smaller than the macroscopic crack length at $N = 1000$, which was 62.5 µm. The point for the macroscopic crack deviated far from the regression line. For this statistical estimation of the maximum crack length, only seven traced areas were examined and those might not be large enough for obtaining an accurate regression line. The crack growth after the initiation also might cause scatter in the Gumbel plot.

From the change in the crack length of the macroscopic crack shown in Fig. 13, the size

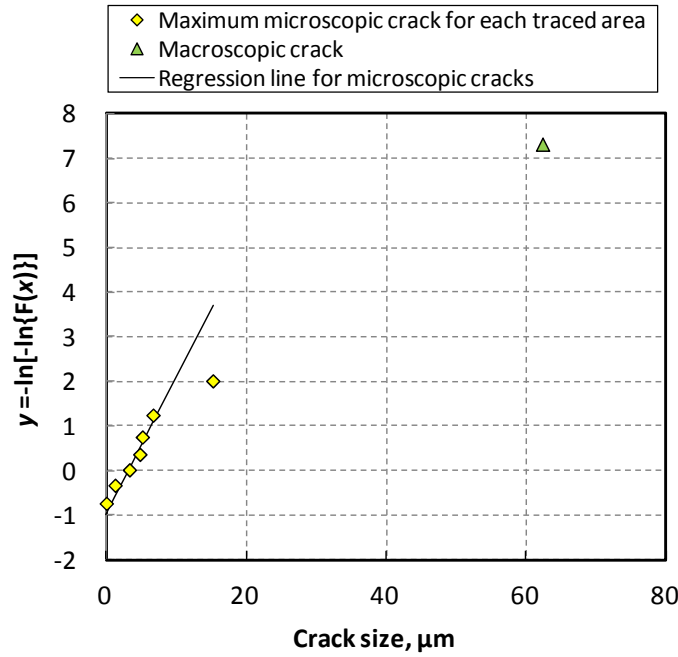


Fig. 15 Gumbel probability plot of the maximum microscopic crack for each traced area and the macroscopic crack at $N = 1000$.

corresponding to $N = 0$ was approximately $30 \mu\text{m}$ and the incubation period (initiation life) seemed to be negligibly small. It should be noted that no coalescence was observed for the macroscopic cracks, although multiple microscopic cracks were observed at some hot spots. Under larger strain range, the enhanced crack initiation may accelerate the crack growth by coalescence of adjacent cracks [38].

4.2 Relationship between main crack growth and fatigue life [23]

Since the initiation life was relatively short and the growth rate of the macroscopic crack was stable, the fatigue life can be deduced by predicting the crack growth without considering the scatter in the growth rate and without assuming the initiation life. The crack growth rate represented by Eq. (3) is expressed in general form as:

$$\frac{da}{dN} = D(\Delta K_e)^m = D(f \Delta \varepsilon \sqrt{\pi a})^m, \quad (4)$$

If the crack size is small enough f can be taken as a constant value. Then, by integrating Eq. (4), the crack depth is obtained by:

$$a = \left\{ D \pi^{\frac{m}{2}} (f \Delta \varepsilon)^m \left(1 - \frac{m}{2} \right) N + a_i^{1-\frac{m}{2}} \right\}^{\frac{2}{2-m}}. \quad (5)$$

By assuming the initial depth a_i , the crack growth can be predicted analytically. When the initiation life was assumed to be zero, the fatigue life is equivalent to the number of cycles necessary to reach the critical depth a_f . Then, fatigue life N_f is obtained as:

$$N_f = \frac{1}{D(f \Delta \varepsilon)^m \pi^{\frac{m}{2}}} \left(\frac{2}{2-m} \right) \left(a_f^{1-\frac{m}{2}} - a_i^{1-\frac{m}{2}} \right). \quad (6)$$

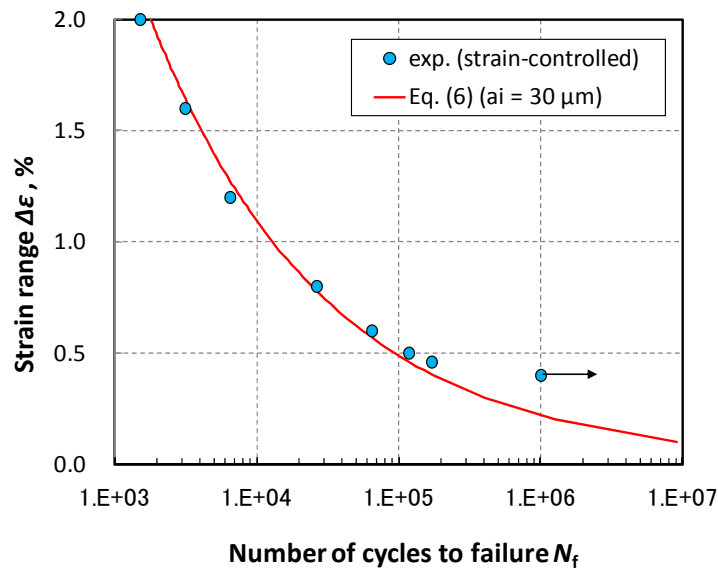


Fig. 16 Fatigue life estimated by crack growth prediction for $a_i = 30 \mu\text{m}$ together with experimental results.

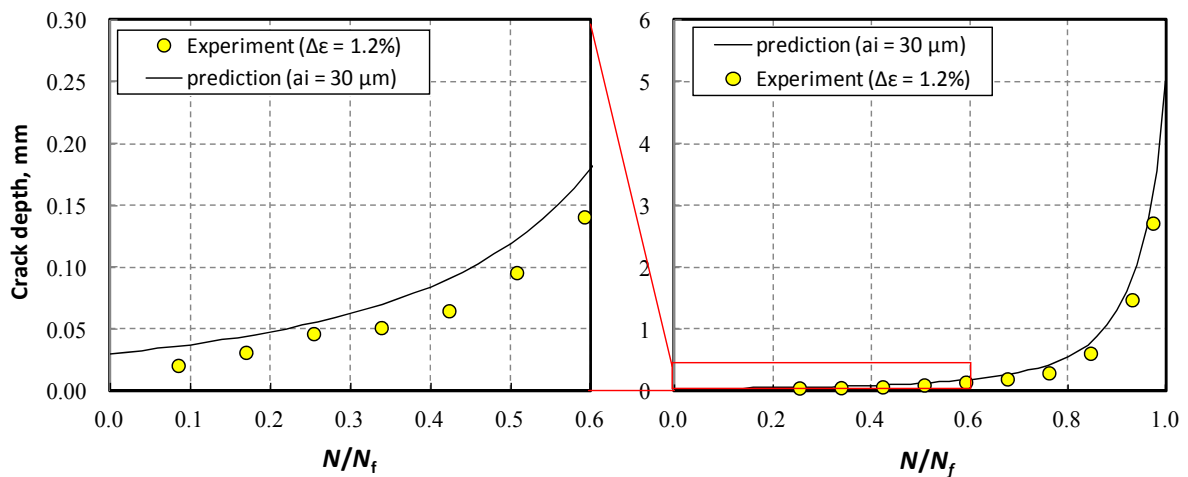


Fig. 17 Change in crack depth obtained by the crack growth prediction ($a_i = 30 \mu\text{m}$).

The fatigue lives estimated by Eq. (6) are shown in Fig. 16 together with the experimental results. The crack growth rate of Eq. (3) and constant $f = 0.723$, which corresponded to $a/R = 0.4$ (R : radius of specimen) [41], was used for the prediction. The initial and critical crack depth were assumed to be $a_i = 30 \mu\text{m}$ and $a_f = 5 \text{ mm}$, respectively. The estimated fatigue lives agreed well with the experimental results except for the unfailed specimen.

4.3 Estimation of fatigue damage from crack size

Figure 17 shows the change in crack depth predicted by Eq. (5). The growth rate of Eq. (3) and $a_i = 30 \mu\text{m}$ and $a_f = 5 \text{ mm}$ were used for the prediction. Eq. (5) could predict the growth of the macroscopic cracks, for which depth was calculated assuming the aspect ratio to be 0.5. According to Eq. (5), the change in crack size against N/N_f was the same under the same initial crack depth regardless of the magnitude of the strain range.

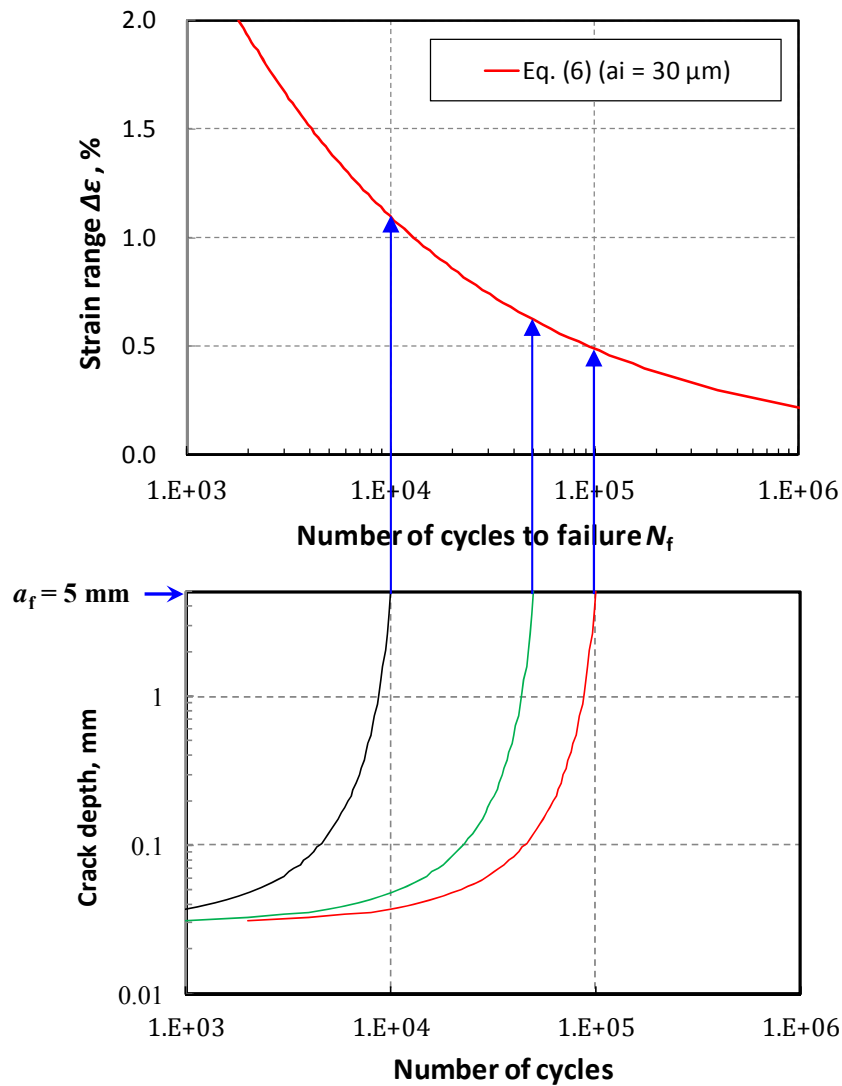


Fig. 18 Normalized initiation life N_i under different definitions of initial crack depth.

Figure 18 shows the correlation between the number of cycles, crack depth and fatigue life. Since the fatigue life could be estimated by the crack growth prediction using Eq. (5), the fatigue damage (N/N_f) and crack size was successfully correlated in Figs. 17 and 18. The number of cycles during plant operation can be obtained from the operation history of each plant. For example, from Fig. 17, it is possible to estimate that remaining life after emergence of the crack of 0.1 mm depth was about $0.5N_f$. The fatigue damage of plant components can be estimated by identifying the crack size. It should be noted that, in general, it is difficult to find a crack with a size less than 1 mm by non-destructive inspection techniques such as ultrasonic testing. A detailed inspection for identifying smaller sizes of crack should be made. SEM observation can find cracks of a few microns without difficulty. The crack growth could be estimated by assuming the stable growth rate without scattering even when the detected crack size was small.

5. Conclusion

In order investigate initiation and growth of small cracks, SEM observations were made for the surface of solution heat-treated Type 316 austenitic stainless steel specimens by interrupting the strain-controlled fatigue test conducted in a room temperature laboratory environment. EBSD measurements were made to correlate the crack initiation to grain boundaries and inhomogeneity of

local deformation. The obtained growth rates were compared with those of macroscopic cracks and the characteristics of the small crack growth were discussed. The results obtained are summarized as follows.

1. By using SEM, small cracks with a size less than a few microns could be observed. There were four typical crack initiation sites: triple point, grain boundary (excluding the twin boundary), twin boundary and intra-grain. The cracks were preferentially initiated from grain boundaries, including twin boundaries and triple points, in the fatigue test of the strain range of 1.2%.
2. The growth rates of small cracks of surface length more than a few tens of microns were stable (without significant scattering in growth rate) and were similar to growth rates of the macroscopic cracks under the same strain intensity factor. Therefore, crack growth could be estimated by assuming the stable growth rate without scattering even when the detected or assumed crack size was small.
3. By assuming the initial depth of 30 μm , the fatigue life and change in crack size could be estimated by predicting the crack growth based on the strain intensity factor.
4. The crack size and fatigue damage was successfully correlated. The remaining life after emergence of the crack of 0.1 mm depth was about $0.5N_f$.

Acknowledgement

The author wishes to acknowledge the experimental support provided by S. Yamahigashi in conducting the crack observations.

References

- [1] ASME: "Rules for Construction of Nuclear Facility Components – ASME Boiler and Pressure Vessel Code Section III", ASME, New York (2000).
- [2] Y. Murakami, K.J. Miller: "What is fatigue damage? A view point from the observation of low cycle fatigue process", *International Journal of Fatigue*, Vol. 27, pp.991-1005(2005).
- [3] M. Kikukawa, K. Ohji, H. Ohkubo, T. Yokoi, T. Morikawa: "Damage and recovery from it in low cycle fatigue", *Transactions of the Japan Society of Mechanical Engineers*, Vol. 38, pp. 8-15 (1972).
- [4] H. Nishitani, T. Morita: "Fatigue Damage in low cycle fatigue of carbon steel specimens", *Transactions of the Japan Society of Mechanical Engineers*, Vol. 39, pp.1711-1719 (1973).
- [5] M. Kamaya: "Fatigue properties of 316 stainless steel and its failure due to internal cracks in low-cycle and extremely low-cycle fatigue regimes", *International Journal of Fatigue*, Vol. 32, pp.1081-1089 (2010).
- [6] M. Kamaya, M. Kawakubo: "Strain-based modeling of fatigue crack growth – An experimental approach for stainless steel", *International Journal of Fatigue*, Vol. 44, pp. 131-140 (2012).
- [7] ASTM: "Standard Test Method for Measurement of Fatigue Crack Growth Rates", ASTM E647-00 (2000).
- [8] A. Fatemi, L. Yang: "Cumulative fatigue damage and life prediction theories: a survey of the state of the art for homogeneous materials", *International Journal of Fatigue*, Vol. 20, pp.9-34 (1998).
- [9] A.H. Noroozi, G. Glinka, S. Lambert: "Prediction of fatigue crack growth under constant amplitude loading and a single overload based on elasto-plastic crack tip stresses and strains", *Engineering Fracture Mechanics*, Vol. 75, pp.188-206 (2008).
- [10] V. Maurel, L. Rémy, F. Dahmen, N. Haddar: "An engineering model for low cycle fatigue life based on a partition of energy and micro-crack growth", *International Journal of Fatigue*, Vol. 31, pp.952-961 (2009).
- [11] A. Carpinteri, M. Paggi: "A unified interpretation of the power laws in fatigue and the analytical correlations between cyclic properties of engineering materials", *International Journal of Fatigue*, Vol. 31, pp.1524-1531 (2009).
- [12] N. Ranganathan, H. Aldroe, F. Lacroix, F. Chalon, R. Leroy, A. Tougui: "Fatigue crack initiation at a notch", *International Journal of Fatigue*, Vol. 33, pp.492-499 (2011).
- [13] K. Tanaka: "Mechanics and micromechanics of fatigue crack propagation", *ASTM STP 1020*, pp.151-183 (1989).
- [14] A.J. McEvily: "The growth of short fatigue cracks: A review", *Material Science Research International*, Vol. 4, pp.3-11 (1998).
- [15] K. Tanaka, T. Hoshide, O. Maekawa: "Surface-crack propagation in plane-bending fatigue of smooth specimen of low-carbon steel", *Engineering Fracture Mechanics*, Vol. 16, pp.207-220 (1982).
- [16] H. Kitagawa, S. Takahashi, C.M. Suh, S. Miyashita: "Quantitative analysis of fatigue process - microcracks and slip lines under cyclic strains", *ASTM STP 675*, pp.420-449 (1979).

- [17] J.R. Haigh, R.P. Skelton: "A strain intensity approach to high temperature fatigue crack growth and failure", *Materials Science and Engineering*, Vol. 36, pp.133-137 (1978).
- [18] S. Suresh: "Crack deflection: Implications for the growth of long and short fatigue cracks", *Metallurgical Transactions*, Vol. 14A, pp.2375-2385 (1983).
- [19] M. Kamaya: "Influence of grain boundaries on short crack growth behavior of IGSCC", *Fatigue & Fracture of Engineering Materials & Structures*, Vol. 27, pp.513-522 (2004).
- [20] M. Kamaya, T. Kitamura: "Stress intensity factors of microstructurally small crack", *International Journal of Fracture*, Vol. 124, pp.201-213 (2003).
- [21] M. Kamaya, T. Kitamura: "A simulation on growth of multiple small cracks under stress corrosion", *International Journal of Fracture*, Vol. 130, pp.787-801 (2004).
- [22] M. Kawakubo and M. Kamaya: "Fatigue life prediction of stainless steel under variable loading (damage factors determining fatigue life and damage evaluation for two-step test)", *Journal of the Society of Materials Science, Japan*, Vol. 60, pp.871-878 (2011).
- [23] M. Kamaya, M. Kawakubo: "Damage assessment of low-cycle fatigue by crack growth prediction (development of growth prediction model and its application)", *Transactions of the Japan Society of Mechanical Engineers. A*, Vol. 78, pp.1518-1533 (2012).
- [24] M. Kamaya: "Measurement of local plastic strain distribution of stainless steel by electron backscatter diffraction", *Materials Characterization*, Vol. 60, pp.125-132 (2009).
- [25] M. Kamaya: "Assessment of local deformation using EBSD: Quantification of accuracy of measurement and definition of local gradient", *Ultramicroscopy*, Vol. 111, pp.1189-1199 (2011).
- [26] M. Kamaya, A.J. Wilkinson, J.M. Titchmarsh: "Measurement of plastic strain of polycrystalline material by electron backscatter diffraction", *Nuclear Engineering and Design*, Vol. 235, pp.713-725 (2005).
- [27] J. F. Nye: "Some geometrical relations in dislocated crystals", *Acta Metallurgica*, Vol. 1, pp.153-162 (1953).
- [28] A.J. Wilkinson, D.J. Dingley, G. Meaden: "Strain mapping using electron backscatter diffraction", in: A. J. Schwartz, M. Kumar, B. L. Adams, D. P. Field (Eds.), "Electron Backscatter Diffraction in Materials Science", Second edition, Springer Science + Business Media, New York, pp. 231-249 (2009).
- [29] D.P. Field, P.B. Trivedi, S.I. Wright, M. Kumar: "Analysis of local orientation gradients in deformed single crystal", *Ultramicroscopy*, Vol. 103, pp.33-39 (2005).
- [30] D. Raabe, Z. Zhao, S.J. Park, F. Roters: "Theory of orientation gradients in plastically strained crystals", *Acta Materialia*, Vol. 50, pp.421-440 (2002).
- [31] M. Calcagnotto, D. Ponge, E. Demir, D. Raabe: "Orientation gradients and geometrically necessary dislocations in ultrafine grained dual-phase steels studied by 2D and 3D EBSD", *Materials Science and Engineering: A*, Vol. 527, pp.2738-2746 (2010).
- [32] A.J. Wilkinson, D. Randman: "Determination of elastic strain fields and geometrically necessary dislocation distributions near nanoindentations using electron back scatter diffraction", *Philosophical Magazine*, Vol. 90, pp.1159-1177 (2010).
- [33] J. W. Kysar, Y. Saito, M. S. Oztop, D. Lee, W. T. Huh: "Experimental lower bounds on geometrically necessary dislocation density", *International Journal of Plasticity*, Vol. 26, pp.1097-1123 (2010).
- [34] M. Kamaya, J. Quinta Da Fonseca, L.M. Li, M. Preuss: "Local plastic strain measurement by EBSD", *Applied Mechanics and Materials*, Vol. 7-8, pp.173-179 (2007).
- [35] J. Man, T. Vystavěl, A. Weidner, I. Kuběna, M. Petrenek, T. Kruml, J. Polák: "Study of cyclic strain localization and fatigue crack initiation using FIB technique", *International Journal of Fatigue*, Vol. 39, pp.44-53 (2012).
- [36] Z. J. Zhang, P. Zhang, L. L. Li, Z. F. Zhang: "Fatigue cracking at twin boundaries: Effects of crystallographic orientation and stacking fault energy", *Acta Materialia*, Vol. 60, pp.3113-3127 (2012).
- [37] P. Zhang, Z. J. Zhang, L. L. Li, Z. F. Zhang: "Twin boundary: Stronger or weaker interface to resist fatigue cracking?", *Scripta Materialia*, Vol. 66, pp.854-859 (2012).
- [38] I. S. Raju, J. C. Newman, Jr.: "Stress-intensity factors for internal and external surface cracks in cylindrical vessels", *Journal of Pressure Vessel Technology*, Vol. 104, pp.293-298 (1982).
- [39] M. Kamaya, T. Kitamura: "Influence of crystal grain on stress intensity factor of microstructurally small cracks", *Journal of Solid Mechanics and Materials Engineering*, Vol. 1, pp.827-841 (2007).
- [40] M. Kamaya and T. Haruna: "Influence of local stress on initiation behavior of stress corrosion cracking for sensitized 304 stainless steel", *Corrosion Science*, Vol. 49, pp.3303-3324 (2007).
- [41] Y. Murakami et al. (eds.): "Stress Intensity Factor Handbook", Volume 2, pp.659-662 (1987).